Polymer 49 (2008) 2461–2470

Contents lists available at ScienceDirect

Polymer

journal homepage: www.elsevier.com/locate/polymer

Tri-block copolymers with mono-disperse crystallizable diamide segments: Synthesis, analysis and rheological properties

A. Arun [a,b,1], R.J. Gaymans [a,*]

[a] University of Twente, P.O. Box 217, 7500AE Enschede, The Netherlands
[b] Dutch Polymer Institute (DPI), P.O. Box 902, 5600 AX Eindhoven, The Netherlands

ARTICLE INFO

Article history:
Received 29 January 2008
Received in revised form 21 March 2008
Accepted 29 March 2008
Available online 8 April 2008

Keywords:
Tri-block
Mono-disperse
Mechanical properties

ABSTRACT

Tri-block copolymers with polyether mid-segments and mono-disperse amide end segments were synthesized, analyzed and some properties studied. The end segment was an aromatic diamide (diaramide, TΦB). The polyether mid-segment was a difunctional poly(tetramethylene oxide) (PTMO, 1000 and 2900 g/mol). In order to increase the soft segment (SS) length, PTMOs were extended with terephthalic groups. The length of the mid-soft segment was varied from 1000 to 20,000 and thereby the concentration of the hard end segment changed from 22 to 3 wt.%. The molecular weight of the tri-block copolymers was determined by NMR and inherent viscosity measurements. The crystallinity of the hard segment was studied by IR and DSC measurements. Temperature modulated IR was carried out to explore the change in crystallinity with temperature. The morphology was investigated by AFM analysis and the thermo-mechanical properties by DMA, whereas the melt rheological behaviour was analyzed by a plate–plate method. The results of the tri-block copolymer were compared with those of a similar multi-block copolymer. The glass transition of the soft phase was low and the melting temperature of the diamide end blocks was high. The crystallinity of the hard end segments in the tri-block was found to be very high (>95%) and remained high until melting. The AFM picture showed crystalline ribbons with a high aspect ratio. Also the modulus at room temperature was relatively high, particularly at low contents of hard end segment. The melt rheological behaviour of a low molecular weight tri-block copolymer revealed a low melt viscosity at high shear rates, and a high viscosity at low shear rates. Moreover, a gelling of the melt was observed with decreasing frequency and this was probably due to agglomeration of the end segments.

1. Introduction

Tri-block copolymers are interesting two phase materials [1,2], and polymers such as styrene–butadiene–styrene (SBS) usually display liquid–liquid demixed phase structures with a dispersed amorphous polystyrene phases. In order to obtain good mechanical properties, the molecular weights of the SBS copolymers should be high and the hard segments should also have high molecular weights; the polystyrene segment length is often on the order of 25,000 g/mol. Due to the high molecular weight, the blocks are often immiscible and this is even in the melt. These SBS tri-block copolymers usually demonstrate low moduli and low maximum use temperatures. Tri-block copolymers with crystallizable end segments have been made from short soft mid-segments (600–3000 g/mol) and long nylon-6 or nylon-11 hard segments [3,4]. The long nylon blocks were phase separated from the soft segments and the nylon blocks were partly crystalline.

Thermoplastic elastomers are the multi-block segmented copolymers with excellent mechanical and thermal properties [1,5]. These multi-block copolymers have short soft and hard segments (1000–3000 g/mol) and had homogenous melts. The hard segments phase separate by crystallization upon cooling and the crystallites provide the copolymers with a low T_g, a relatively high modulus at room temperature and high maximum use temperature. If the hard segments (HS) are mono-disperse in length the copolymer has a lower soft segment T_g and a sharper hard segment melting transition [6–18]. The mono-disperse segments crystallize fast and almost completely, and as a result, the soft phase contains very little dissolved hard segments. The mono-disperse HS have crystallites with nano-ribbon-like structures with high aspect ratios (i.e., 300–1000) [11–13,15,17,19]. When the HS are truly mono-disperse the modulus is from room temperature to near the HS melting temperature almost independent of temperature. If the mono-disperse HS contain amide segments, H-bonding is with the two neighbouring chains in the crystal and, ribbon-like H-bonded

* Corresponding author.
E-mail address: r.j.gaymans@tnw.utwente.nl (R.J. Gaymans).
[1] Present address: Government Arts College, Tiruvannamalai, Tamil Nadu, India.

0032-3861/$ – see front matter © 2008 Elsevier Ltd. All rights reserved.
doi:10.1016/j.polymer.2008.03.049

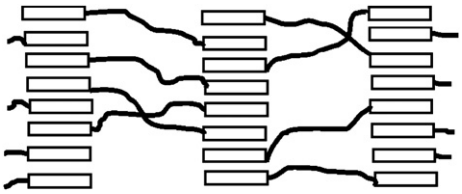

Fig. 1. A schematic representation of a tri-block copolymer with mono-disperse crystallized end segments.

structures were formed. These nano-ribbon-like crystallites had high aspect ratios. In the H-bonding direction, the crystallites can be as long as 1000 nm. These nano-ribbon crystallites are the physical crosslinks for the soft phase and also reinforce the soft phase.

Tri-block copolymer of telechelic mid-segments and short mono-disperse H-bonding end segments is a novel concept. The H-bonding end segments, e.g. ureidopyrimidinone (UP) units, are able to form dimer interactions [20–25], and due to this dimer H-bonding, the low molecular weight copolymers become non-covalently bonded to supramolecular polymers with properties of a high molecular weight polymer [22,26–28]. The melting temperature of copolymers comprising these dimer interactions is low, as is the moduli of the copolymers.

It would be interesting to study tri-block copolymers with mono-disperse amide end segments. As a result of the amide end segments, H-bonding should be possible with the two neighbouring chains in the crystal, and in that way long H-bonded ribbon-like crystalline structures are expected to be formed. As the crystallinity of the mono-disperse amide segments is normally very high, a network formation is expected to take place with these tri-block copolymers. A crystallization of all the end blocks leads to all the mid-blocks becoming part of a network (Fig. 1). Since the crystallizable segments in a tri-block copolymer are represented by the chain ends, the flexibility of the material is expected to be higher than if the crystallizable units were positioned in the chain.

It would be interesting to study the properties of tri-block copolymers with short mono-disperse mono-functional amide end segments and varying lengths of the mid-segment. This approach would lead to two parameters being varied: the molecular weight of the copolymer and the hard segment content. Consequently, it might be possible to obtain tri-block copolymers with relatively low molecular weights and good dimensional stability as well as low melt viscosities. Such properties can be compared to those of high molecular weight multi-block copolymers. The present paper reports on the synthesis and properties of aramide–(polytetramethylene oxide)–aramide tri-block copolymers. The short mono-functional diaramide hard segments (TΦB-monoester) were synthesized in the first step and subsequently used in the preparation of the tri-block copolymers (Fig. 2b). The TΦB-monoester had a structure very similar to that of the bifunctional diaramide (TΦT-diester) (Fig. 2a) segment used by Niesten et al. [10] for segmented multi-block copolymers.

In the preparation of the tri-block copolymers, poly(tetramethylene oxide) (PTMO) with molecular weights of either 1000 or 2900 g/mol was used. The $PTMO_{2900}$ had a relatively high melting temperature and could be readily strain crystallized [17,29]. The soft segment (SS) length was further increased by extending the PTMO with terephthalic units up to a total length of 20,000 g/mol [11,17,30]. The used polyether segments had a normal length distribution (~2). The synthesis of these tri-block copolymers was thus investigated and the crystallization rate and crystallinity of TΦB segments, the morphology of the crystallites, the thermo-mechanical behaviour and the melt rheological behaviour were explored.

2. Experimental

2.1. Materials

Dimethyl terephthalate (DMT), and *N*-methyl-2-pyrrolidone (NMP) were purchased from Merck. Tetraisopropyl orthotitanate ($Ti(i\text{-}OC_3H_7)_4$) was also obtained from Merck and was diluted in anhydrous *m*-xylene (0.05 M), from Fluka. Deuterated trifluoroacetic acid (TFA-*d*), phenol, 1,1,2,2-tetrachloroethane and 1,1,1,3,3,3-hexafluoroisopropanol (HFIP) were purchased from Aldrich Chemicals. Poly(tetramethylene oxide) (PTMO, $M_n = 1000$ and 2900 g/mol) was generously donated by DuPont. Irganox 1330 (1,3,5-trimethyl-2,4,6-tris(3,5-di-*t*-butyl-4-hydroxybenzyl)benzene) was obtained from CIBA, and 4′-aminobenzanilide was purchased from Aldrich. Methyl(4-chlorocarbonyl)benzoyate (MCCB) was obtained from Dalian (No. 2 Organic Chemical Works, China). All chemicals were used as-received.

2.2. Synthesis of TΦB-monomethyl ester (Scheme 1)

MCCB (3 g, 0.015 mol) was dissolved in 25 mL of NMP at room temperature in a 250 mL flask fitted with a mechanical stirrer, a nitrogen inlet, and a calcium chloride tube. 4′-Aminobenzanilide (3.4 g, 0.016 mol), previously dissolved in 125 mL of NMP was added. After 2 h, methanol (25 mL) was added and stirring was carried out for another 2 h. The reaction mixture was filtered and washed with hot toluene, and twice in hot acetone. The product TΦB-monomethyl ester was subsequently dried in a vacuum oven at 70 °C and the yield obtained was 60%.

2.3. General procedure for the synthesis of tri-block copolymer (Scheme 2)

The tri-block copolymers that were synthesized are presented in Scheme 2. The preparation of TΦB–$(PTMO_{2900}–T)_{9000}$–TΦB is given as an example. The reaction was carried out in a 250 mL stainless steel vessel with a nitrogen inlet and a mechanical stirrer. The reactor was charged with TΦB-monomethyl ester (3 g, 0.008 mol), $PTMO_{2900}$ (34.8 g, 0.012 mol), DMT (1.55 g, 0.008 mol), 1 wt.% (SS) of Irganox 1330 (0.364 g), the catalyst solution (1.2 mL of 0.05 M $Ti(i\text{-}OC_3H_7)$ in *m*-xylene), and 75 mL of NMP under nitrogen flow. The stirred reaction mixture was heated to 180 °C for 30 min and the temperature was subsequently raised step-wise to 250 °C over a time period of an hour. At 250 °C the reaction mixture was

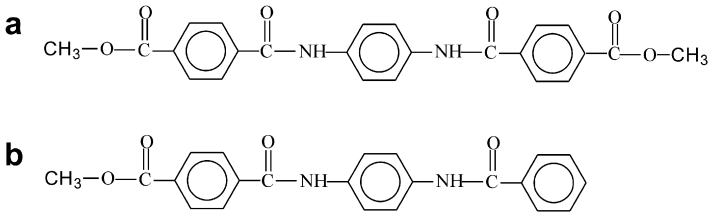

Fig. 2. Chemical structures of (a) TΦT-diester and (b) TΦB-monoester.

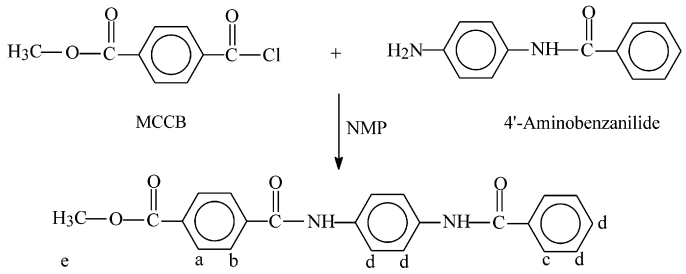

methyl 4-({[4-(benzoylamino)phenyl]amino}carbonyl)benzoate (TΦB-mono methyl)

Scheme 1. The synthesis of TΦB-monomethyl.

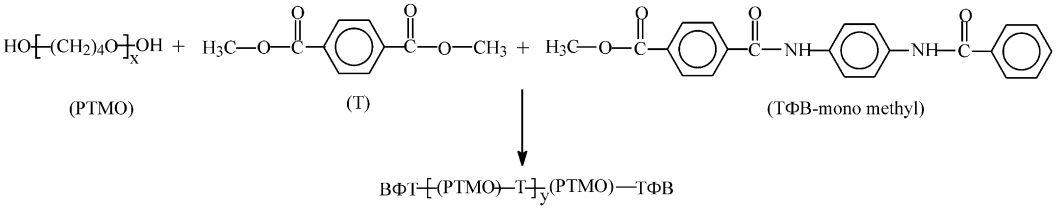

Where,

1a,	$PTMO_{1000}$	and	Y = 2000	2a,	$PTMO_{2900}$	and	Y = 0
1b,	$PTMO_{1000}$	and	Y = 5000	2b,	$PTMO_{2900}$	and	Y = 3000
1c,	$PTMO_{1000}$	and	Y = 9000	2c,	$PTMO_{2900}$	and	Y = 6000
1d,	$PTMO_{1000}$	and	Y = 19000	2d,	$PTMO_{2900}$	and	Y = 17000

Scheme 2. The synthesis of the tri-block copolymer.

stirred for 2 h, after which the pressure was carefully reduced ($P < 20$ mbar) to distil-off the NMP. The pressure was further reduced to <0.3 mbar and reacted for 1 h after which the reaction mass was cooled while maintaining the low pressure. The copolymer was transparent with a yellowish hue. The copolymer was dried overnight in vacuum at 70 °C before further use.

2.4. Analysis

2.4.1. Inherent viscosity

The inherent viscosity of the polymers at a concentration of 0.1 g/dL in a 1:1 (molar ratio) mixture of phenol–1,1,2,2-tetrachloroethane at 25° C was determined using a capillary Ubbelohde 0C.

2.4.2. MALDI-TOF

Mass spectroscopy was performed using a voyager-DE-RP MALDI-TOF mass spectrometer equipped with delayed extraction. Mass spectra were obtained in reflection mode with a 337 nm UV nitrogen laser producing 3 ns pulses. Samples were dissolved in 10 μL of triflouroacetic acid and 30 μL of water/acetonitrile (equimolar mixture) solution. One milligram of dihydroxybenzoic acid (DHB) was added to the solution as the matrix. One microliter of the solution was placed on a gold 100-well plate. The solvent was evaporated and the plate was transferred to the mass spectrometer.

2.4.3. ^1H NMR

Proton NMR spectra were recorded on a Bruker AC 300 spectrophotometer at 300.1 MHz. Deuterated triflouroacetic acid (TFA-*d*) was used as the solvent. All the polymers and TΦB were characterized by the ^1H NMR technique.

2.4.4. FT-IR

Infrared spectra were recorded using Nicolet 20SXB FT-IR with a resolution of 4 cm^{-1}. Samples were prepared by adding a droplet of a polymer solution (HFIP (1 g/L)) on a pressed KBr pellet and the measurements were carried out at room temperature. Solution cast polymer films (0.05 g/mL in HFIP) of <10 μm thicknesses, placed in-between two KBr pellets, were used for the temperature dependent FT-IR analyses. These measurements were recorded at temperatures between room temperature and 200 °C under a helium flow. The degree of crystallinity (X_c) of the rigid segments in the polymers was estimated with the following equations:

$$X_c\text{FT-IR} = \frac{\text{crystalline amide peak}}{\text{amorphous} + \text{crystalline amide peak}} = \frac{\lambda_{25\,^\circ\text{C}(1643\ \text{cm}^{-1})}}{a \times \lambda_{25\,^\circ\text{C}(1680\ \text{cm}^{-1})} + \lambda_{25\,^\circ\text{C}(1643\ \text{cm}^{-1})}} \quad (1)$$

The heights of the amorphous and crystalline amide peaks are related by a factor *a*, which can be calculated according to:

$$a = \frac{\text{decrease of crystalline peak}(25\,^\circ\text{C} - \text{melt})}{\text{increase of amorphous peak}(25\,^\circ\text{C} - \text{melt})} = \frac{\lambda_{25\,^\circ\text{C}(1643\ \text{cm}^{-1})} - \lambda_{\text{melt}(1643\ \text{cm}^{-1})}}{\lambda_{\text{melt}(1680\ \text{cm}^{-1})} - \lambda_{25\,^\circ\text{C}(1680\ \text{cm}^{-1})}} \quad (2)$$

2.4.5. Atomic force microscopy (AFM)

AFM measurements were carried out with a nanoscope IV controller (Veeco) operating in tapping mode. The AFM was equipped with a J-scanner with a maximum size of 200 μm^2. Si-cantilevers (Veeco) were used to obtain height and phase images. The amplitude in free oscillation was 5.0 V. The operating set point

value (A/A_o) was set to a relatively low value of 0.7. Scan sizes were 1–3 μm^2 to obtain the best contrast. Solvent cast samples of ~20 μm thick were prepared from a 3 wt.% solution in TFA.

2.4.6. Differential scanning calorimetry (DSC)

DSC spectra were recorded on a Perkin–Elmer DSC7 apparatus, equipped with a PE7700 computer and TAS-7 software. A dried sample (2–5 mg) was heated at a rate of 20 °C/min. The samples were heated to 30 °C above their melting temperature, held at that temperature for 3 min before being cooled. For the TΦB starting material, the onset of the melting peak of the first heating scan was taken as the melting temperature and the peak area was used to calculate the melting enthalpy. For the polymers, the second heating scans were used for determining the melting temperatures. The melting temperature (T_m) was taken as the temperature of the maximum of the endotherm. The first cooling curve was used to determine the crystallization temperature, which was taken as the onset of crystallization. The undercooling ($\Delta T = T_m - T_c$) was calculated and used as a measure of the rate of crystallization.

2.5. Testing

2.5.1. Injection moulding

Test specimens, i.e., bars of 70 × 9 × 2 mm^3, were prepared by processing on an Arburg H manual injection moulding machine. In the case of mono-dispersed amide segments, the barrel temperature was set to 40–50 °C above the melting temperature of the polymer (as determined by DSC). The injection moulded test bars were stored at room temperature for about 2 days before analysis. All the samples were dried overnight in vacuum at 70 °C before use.

2.5.2. Dynamic mechanical analysis (DMA)

The storage (G') and loss (G'') moduli as functions of temperature were measured on injection moulded test bars (70 × 9×2 mm^3) using a Myrenne ATM3 torsion pendulum at a frequency of 1 Hz. The samples were first cooled to −100 °C and subsequently heated at a rate of 1 °C/min and 0.1% strain. The glass transition temperature was determined as the maximum of the loss modulus. The flow or softening temperature (T_{flow}) was defined as the temperature where the storage modulus reached 0.5 MPa. The flex temperature (T_{flex}) was defined as the temperature at the intersection of the tangents at the start of the rubber plateau region. The decrease in storage modulus of the rubbery plateau with increasing temperature was quantified by $\Delta G'$ and was calculated from:

$$\Delta G' = \frac{G'_{(25\,^\circ C)} - G'_{(T_{flow}-25\,^\circ C)}}{G'_{25\,^\circ C}} \times \frac{1}{\Delta T} \quad (\%/^\circ C) \tag{3}$$

Here, ΔT is described as the temperature range: ($T_{flow} - 50$ °C) – 25 °C.

2.5.3. Melt rheology

Rheological measurements were carried out on a Paar Physica UDS200 rheometer with a Paar Physica TC 20 temperature control unit. A parallel-plate set up with a fixed EHH-TEK 350 plate and rotating MP 306 plate was used. The diameter of the upper plate was 25 mm and the gap between the two parallel plates was 0.5 mm. The Paar Physica software was used for all the rheology calculations. Initially, the copolymer was allowed to reside between the two parallel plates at a set temperature for 5 min. A dynamic frequency sweep was then performed on the copolymer at 1% strain.

3. Results and discussion

Tri-block copolymers were synthesized from PTMO-based dihydroxyl soft segments (SS) and monoester diamide units (TΦB) using the one-pot synthetic procedure (cf. Scheme 2). The PTMO-based soft segments comprised either $PTMO_{1000}$ or $PTMO_{2900}$. In order to increase the SS length, the $PTMO_{1000}$ or $PTMO_{2900}$ segments were extended with terephthalic acid groups to $(PTMO_{1000}–T)_y$ and $(PTMO_{2900}–T)_y$. In this way, the molecular weight of the mid-soft segment (y) could be increased from 1000 to 20,000 g/mol without much affecting the properties of the soft phase [17]. $PTMO_{2900}$ was more crystalline than $PTMO_{1000}$ and displayed a stronger strain hardening behaviour upon stretching. The semi-crystalline copolymers were transparent in the melt as well as in the solid state.

3.1. Synthesis of the monoester diamide TΦB

TΦB was synthesized using MCCB and 4′-aminobenzanilide according to the procedure given in Section 2. The purity of the compound was studied by ^1H NMR. The chemical shifts and their integral values are given in Table 1.

The purity of the TΦB-monomethyl ester was calculated from the integral values of the c and b peaks. The purity of the TΦB was found to be very high (>99%, within the error of NMR), and was further characterized by MALDI-TOF. Three peaks were observed in the MALDI-TOF spectra of TΦB: at 375, 396 and 412, corresponding to the molecular ion (M^+), $M^+ + Na$ and $M^+ + K$, respectively. According to the MALDI-TOF, the TΦB was found to be pure. The IR spectrum of TΦB at the room temperature showed a carbonyl peak of the amide I at 1648 cm^{-1} (strong) and of the ester at 1718 cm^{-1}. The hydrogen bonded νN–H region displayed a peak at 3341 cm^{-1}. The amide IR carbonyl band of TΦB-monomethyl was found at a similar wavelength to BΦB (1645 cm^{-1}), and TΦT-dimethyl (1648 cm^{-1}), thus similarly suggesting a similar strong H-bonding and a similar dense packing. The melting behaviour (and enthalpy of melting) of the TΦB was studied by DSC (Fig. 3).

The melting point from the first heating of the TΦB was at 316 °C ($\Delta H_m = 100$ J/g) and that from the second heating was at 301 °C ($\Delta H_m = 92$ J/g). Surprisingly, the melting temperature of the TΦB was 316 °C, while the BΦB and TΦT-dimethyl had respective melting temperatures of 343 and 371 °C [31,32]. Also the heat of fusion for BΦB and TΦT-dimethyl, i.e., 198 and 334 J/g, was higher. The asymmetric structure of TΦB may have influenced the packing and with that the melting temperature and the heat of fusion. The stacking in the crystalline state of TΦB-monomethyl can be either parallel or anti-parallel (Fig. 4).

The structure is expected to be less densely packed in the anti-parallel stacking as a result of the methyl ester groups, although the distance in the H-bonding direction might be similar.

3.2. Synthesis of tri-block copolymers

The tri-block copolymers were synthesized by a condensation reaction between the polyether prepolymers and the ester of the TΦB segment (Scheme 2). The molecular weight of the soft segment

Table 1
Chemical shifts and integral values of TΦB

Peak	Chemical shift δ (ppm)	Type	Number of protons	Integral value
a	8.3	Doublet	2	2
b	8.1	Doublet	2	2
c	7.9	Doublet	2	1.98
d	7.6–7.8	Multiplet	7	7.05
e	4.1	Singlet	3	3.04

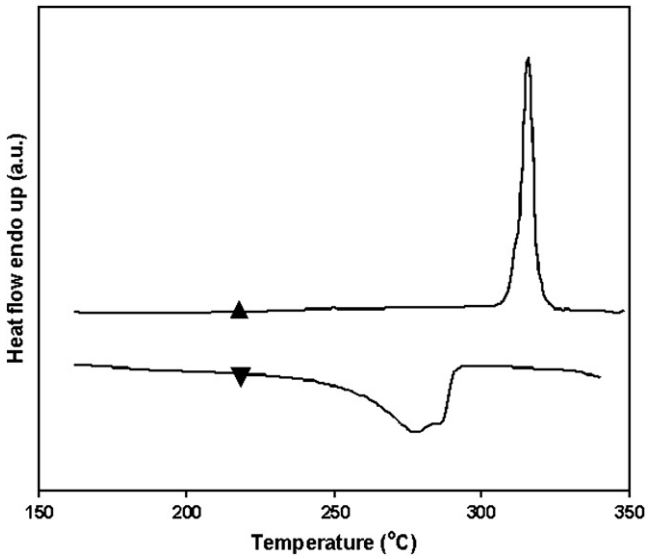

Fig. 3. DSC traces of the first heating (▲) and the cooling (▼) runs of TΦB.

was increased by extending the PTMO segments with terephthalic groups. Previous results from our group have shown that the terephthalic extender increased the soft segment glass transition temperature by only 5 °C [11,17,30]. In this way, the mid-soft segment length could be varied from 1000 to 20,000 g/mol and, thus, the percentage of hard end segments was decreased from 23 to 3 wt.%. Furthermore, the mole fractions of hard and soft segments incorporated in the copolymer were estimated by NMR analysis [10]. The peaks at 7.6–7.8 ppm (7 protons) and 1.9 ppm (4 protons) represented the hard and soft segments, respectively. Since the two peaks were well distinct from each other, the integral values of these two peaks could be conveniently taken for determining the composition of the copolymer. The following equations were used for this calculation, assuming that m_1 and m_2 (or $1 - m_1$) were the mole fractions of soft and hard segments in the copolymer chain, respectively.

$$C = \frac{\text{integral value of } C - CH_2 - CH_2 - C \text{ proton}(I_s)}{\text{integral value of aromatic proton}(7.6 - 7.8 \text{ ppm})\,(I_h)} \quad (4)$$

$$C = \frac{56m_1}{7(1-m_1)} \text{ (for PTMO}_{1000}\text{) and}$$
$$C = \frac{160m_1}{7(1-m_1)} \text{ (for PTMO}_{2900}\text{)} \quad (5)$$

(Since $PTMO_{1000}$ and $PTMO_{2900}$ consisted of 14 and 40 tetramethylene units respectively.)

Upon simplification we get,

$$m_1 = \frac{7C}{56+7C} \text{ (for PTMO}_{1000}\text{) and}$$
$$m_1 = \frac{7C}{160+7C} \text{ (for PTMO}_{2900}\text{)} \quad (6)$$

The mole fraction in the feed and the mole fraction in the copolymer chain calculated through ^{1}H NMR are presented in Table 2.

From Table 2, it is evident that all the TΦB units were incorporated in the polymer chain thereby producing the desired tri-block copolymers. The inherent viscosities were also measured (Table 2). As the molecular weight increased, the inherent viscosity also increased and this increase was linear at low molecular weights (Fig. 5).

On combining the results of inherent viscosity and the NMR calculations, it was clear that the formed copolymers were tri-block copolymers with the expected molecular weights.

3.3. Morphology of tri-block system

The asymmetric TΦB segments can be arranged in the crystalline state in either a parallel or an anti-parallel stacking (Fig. 4). Of course, it is also possible for a mixture of parallel and anti-parallel stacking to take place. Since the SS are long segments, a network structure formation is possible with both the parallel and the anti-parallel stacking.

An IR spectrum of the tri-block copolymer at 25 °C showed a peak centred at 1643 cm^{-1} (Fig. 6). Upon increasing the temperature, this peak decreased in intensity and the broad amorphous amide carbonyl peak observed at 1680–1686 cm^{-1} was increased. The peak at 1643 cm^{-1} was at a lower wavelength as compared to the monomethyl TΦB (1648 cm^{-1}), and the TΦB end segments thus displayed a somewhat stronger H-bonding in the crystalline phase.

The morphology of the TΦB end segment crystallites was studied by AFM. The $PTMO_{2900}$ segments in this copolymer had in a DSC experiment a T_m of 25 °C (Table 3), however, in a static test a lower T_m is expected. Thus during analysis of this sample crystalline PTMO was not expected to be present. In the AFM micrograph of sample **2a** white ribbons can be observed, which were the crystallized hard segments (Fig. 7).

In the studied plane, the tri-block copolymer displayed ribbon-like structures. Since the AFM picture was related to the surface morphology, the length of the crystalline ribbons was very difficult to determine. However, the visible length of the ribbons was 1000 nm. With an extended length of the TΦB segment of about 2 nm, the aspect ratio of the ribbons was at least 500. As the ribbons were very small in both thickness and width direction, these semi-crystalline copolymers were transparent, and no birefringence could be observed with optical microscopy. Similar ribbon-like structures have been seen for multi-block segmented block copolymers [13,15,17–19].

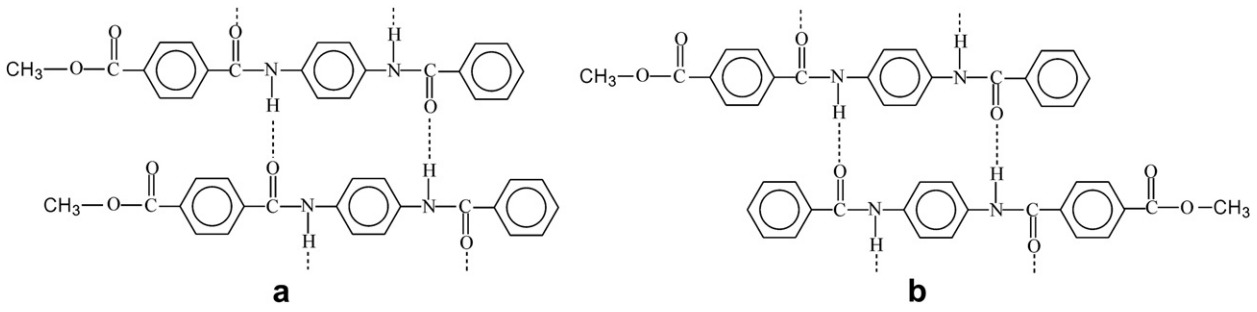

Fig. 4. The TΦB-monomethyl stacking in (a) a parallel or (b) an anti-parallel fashion.

Table 2
The composition of the tri-block copolymers

Sample code	% of TΦB	η_{inh} (dL/g)	Cal. mol. wt.[a] (g/mol)	Feed mol. fraction[b] (m_1)	Integral value		$C = I_s/I_h$	Mol. fraction in copolymer[c] (M_1)
					I_s	I_h		
$PTMO_{1000}$								
1a	22	0.3	2800	0.50	60.16	7.77	7.74	0.49
1b	10	0.6	6200	0.71	149.86	7.36	20.36	0.72
1c	6	0.7	10,700	0.82	47.08	0.73	64.50	0.82
1d	3	1.1	20,900	0.90	254.8	6.91	36.88	0.89
$PTMO_{2900}$								
2a	18	0.4	3600	0.33	89.75	7.55	11.89	0.34
2b	10	0.6	6600	0.50	167.35	7.44	22.49	0.50
2c	7	0.9	9600	0.60	288.96	8.00	36.12	0.61
2d	3	1.4	21,700	0.78	562.67	6.72	83.73	0.78

Subscript "s" refers to the soft segment and "h" refers to the TΦB (hard) segment.
[a] M_n calculated from feed composition.
[b] Mole fraction of PTMO in the feed.
[c] Mole fraction of PTMO according to NMR.

3.4. Thermal properties of tri-block copolymers

The thermal properties of the tri-block copolymers were studied by DSC, temperature modulated IR spectroscopy and DMA. A typical DSC thermogram is given in Fig. 8 and the results are summarized in Table 3.

The melting of the SS of the $PTMO_{1000}$-based polymers started at 9 °C and increased slightly with increasing SS length. Moreover, the crystallization temperature of SS decreased with increasing SS length (Table 3). For the $PTMO_{2900}$-based polymer, the melting of the soft segment was around 25 °C and increased slightly upon increasing the SS length. Here again, the crystallization temperature of the SS decreased with increasing SS length. The decrease in the crystallization temperature was believed to have been due to the terephthalic groups disturbing the crystallization.

With DSC, the amide segment melting temperatures and heats of fusion could only be determined at HS concentrations higher than 10 wt.%. For the samples **1a** and **2a**, two HS melting and crystallization transitions could be observed. Two transitions are often observed for semi-crystalline polymers [33]. The lower transition has been explained as being due to a solid state transition. The melting and crystallization peaks were shallow and the heats of fusion were difficult to determine. The observed melting enthalpies for **1a** and **2a** copolymers were 73–96 J/g for their HS. For the TΦB-monomethyl ester, a heat of fusion of 92 J/g (second heating scan) was measured. Based on this heat of fusion, the HS crystallinity of **1a** and **2a** samples must have been high (>80%).

A measure of the crystallization rate was determined dynamically with DSC by measuring the crystallization temperature as a function of the cooling rate. The sensitivity of the crystallization towards the cooling rate was proposed by Nadkarni et al. [34]. The variation of supercooling ΔT ($T_{m,\,peak} - T_{c,\,peak}$) with cooling rate ($\lambda$) can be fitted to a linear equation,

$$\Delta T = P\lambda + \Delta T^0$$

A plot of ΔT versus λ gives a straight line with the intercept of ΔT^0 and the slope of P. An idea of the inherent crystallizability of the polymer can be obtained from the value of the zero cooling rate (ΔT^0). This value is related to the thermodynamic driving force for nucleation. The slope P (min) is a process sensitivity function and accounts for kinetic effects. The crystallization behaviour of the polymers **1a** (0.27 dL/g) and **2a** (0.37 dL/g) was studied with different cooling rates (Fig. 9).

As the cooling rate increased, the onset crystallization temperature decreased and the peak broadened. Extrapolating the crystallization temperatures to cooling rate zero (T^0) gave 244 and 236 °C, and the observed melting temperatures (at 20 °C/min) were, respectively, 248 and 239 °C. With these values, the undercooling temperatures (ΔT^0) could be calculated (Table 4). The ΔT^0 values for the TΦB were extremely low as compared to other polymer systems (Table 4), thus suggesting a very fast

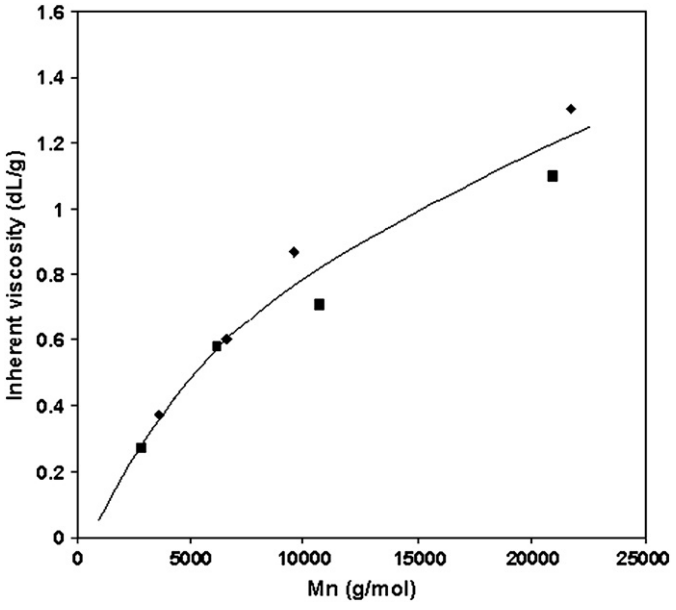

Fig. 5. The inherent viscosity versus $M_{n\ from\ feed}$: ◆, $PTMO_{2900}$; ■, $PTMO_{1000}$.

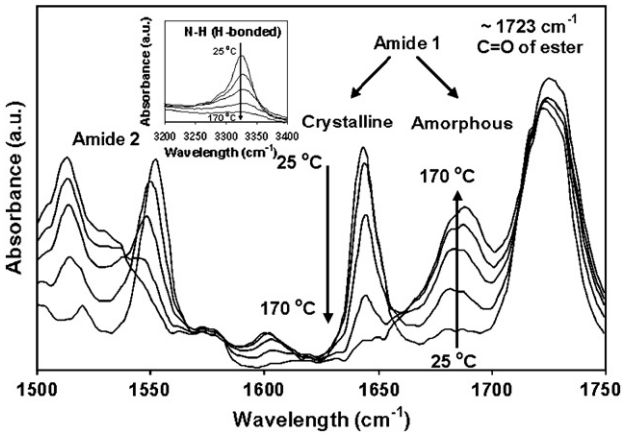

Fig. 6. The effect of temperature on the IR spectrum of $\eta = 1.4$ dL/g polymer (**2d**). Inset: H-bonded N–H region.

Table 3
Inherent viscosities, DSC and DMA results of the TΦB-based tri-block copolymer

Sample code	Mol. wt. (g/mol)	TΦB (wt.%)	η_{inh} (dL/g)	FT-IR	DSC					DMA			
				X_c (HS) (%)	$T_{m,s}$ (°C)	$\Delta H_{m,s}$ (J/g$_{SS}$)	$T_{m,h}$ (°C)	$\Delta H_{m,h}$ (J/g$_{HS}$)	$T_{c,s}$ (°C)	T_g (°C)	T_{flow} (°C)	$\Delta G'$ (%/°C)	$G'_{30\,°C}$ (MPa)
$PTMO_{1000}$													
1a	2800	22	0.3	>95	9	7	248	96	–	−70	245	0.2	39
1b	6200	10	0.6	>95	11	20	179	33	−50	−65	175	0.2	11
1c	10,700	6	0.7	94	14	32	–	–	−33	−65	150	0.2	6
1d	20,900	3	1.1	>95	15	33	–	–	−33	−65	135	0.3	4.5
$PTMO_{2900}$													
2a	3600	18	0.4	>95	25	36	239	73	−27	−75	230	0.2	29
2b	6600	10	0.6	>95	29	41	–	–	−20	−75	175	0.2	10
2c	9600	7	0.9	>95	28	40	–	–	−17	−75	160	0.2	8
2d	21,700	3	1.4	93	28	44	–	–	−15	−75	130	0.5	4

Subscript "s" refers to soft segment and "h" to TΦB (HS).

crystallization of the TΦB and TΦT segments, and also the rate-dependent crystallization parameter (P) was lower than in other polymer systems (Table 4). The very low ΔT values were possibly due to an ordered arrangement of the hard segments in the melt.

FT-IR spectroscopy is a powerful tool for studying the crystallinity of the amide groups in a (co)polymer. It was thus used to study the crystallinity on the amide carbonyl bands that were sensitive to crystalline order. The crystalline aromatic amide carbonyl band was at 1644–1650 cm^{-1} and the broad amorphous carbonyl band at 1660–1690 cm^{-1}. The crystallinities were determined according to Eq. (1) (Table 3), and the crystallinities of the TΦB segments were all very high (>90%). Also studied was the temperature dependent IR spectrum of the TΦB-based copolymer **2d**, which had an inherent viscosity of 1.4 (Fig. 6). The change in crystallinity of the amide groups in a heating–cooling cycle was determined (Fig. 10).

The crystallinity was high at room temperature and remained fairly high up to the melting temperature, which was followed by a sharp drop in the melting transition (at about 130 °C). The crystallinity had fully disappeared at about 170 °C. On subsequent cooling, the crystallinity recovered almost completely, with only a small temperature lag as compared to the heating curve. This small temperature lag suggested a fast crystallization.

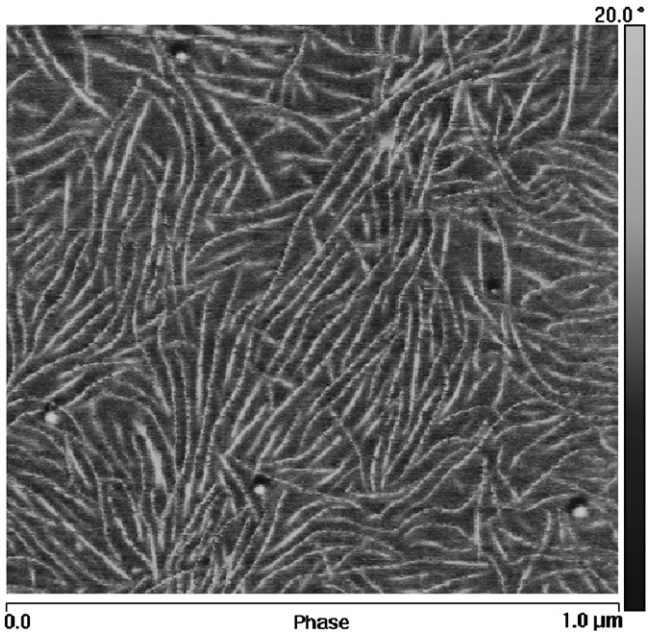

Fig. 7. Phase image of an AFM micrograph of the tri-block (**2a**) containing 3 wt.% of HS.

3.5. DMA

The DMA thermograms of the tri-block copolymers displayed three transitions: the glass transition of PTMO, the melting transition of PTMO and the melting transition of TΦB (Fig. 11).

The T_g of the PTMO phase was found to be around −70 °C, which was a very low value. This suggests that the concentration of dissolved TΦB segments in the polyether phase must have been very low due to the high crystallinity of the TΦB segments. The flex temperature, the melting temperature of PTMO, increased with SS length and was higher for the $PTMO_{2900}$ series (Table 3). The $PTMO_{2900}$ series thus had both a higher crystallinity and a higher SS melting temperature. These tri-block copolymers displayed a long temperature-independent rubbery plateau, which is typical of copolymers with mono-disperse crystallizable segments [6–18]. The thermal stability of the crystallizable segments was quantified by the $\Delta G'$ value, and was found to be low for all copolymers (Table 3). Very few TΦB segments melted at a temperature lower than the melting temperature. The flow temperature of these polymers was sharp and increased with increasing TΦB content in the polymer (or with decreasing soft segment length). The flow temperatures corresponded to the melting temperatures as measured by DSC (Table 3). A sharp T_{flow} was due to a narrow melting transition, typical for mono-disperse HS resulting in crystallites of uniform thickness. The flow temperature (melting temperature) decreased with increasing SS content. This decrease in T_m was due to the solvent effect of the

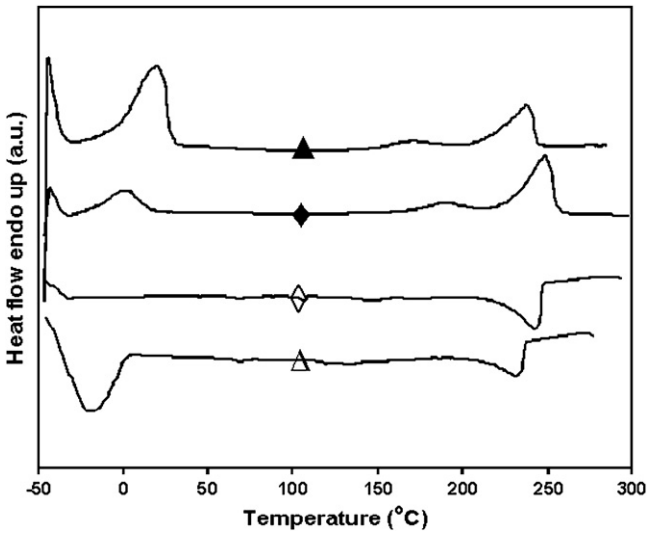

Fig. 8. Heating (closed symbol) and cooling (open symbol) curves of the copolymers **1a** (◆) and **2a** (▲).

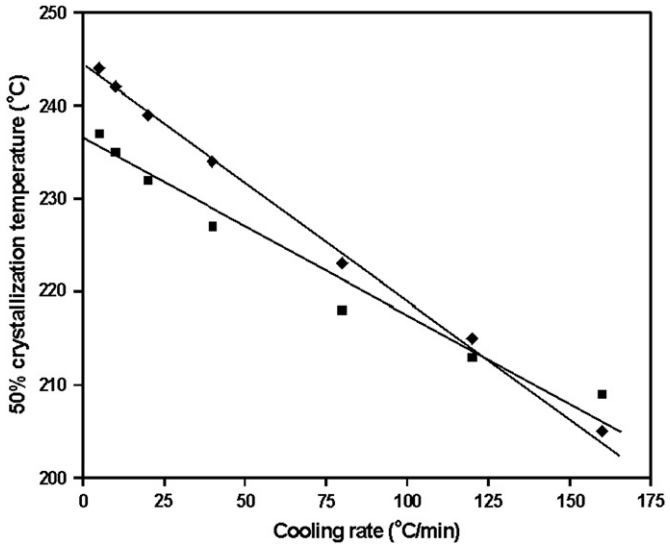

Fig. 9. The effect of cooling rate on the temperature for 50% crystallization: ◆, **1a**; ■, **2a**.

Table 4
A comparison of slope "*P*" and intercept "ΔT^{0}" for several polymers

Sample name	*P* (min)	ΔT^{0} (°C)	Crystallinity (%)	
			DSC	IR
1a	0.25	4	>95	>95
2a	0.18	3	>80	93
Nylon-4,6 [35,36]	0.28	30	55	–
Nylon-6 [35,36]	0.55	40	35	–
PBT [37,38]	0.40	55	42	–
PET [37]	1.30	70	28	–

SS as proposed by Flory [39]. The melting transitions of the tri-block copolymers were on average 20 °C higher than those of the multi-block copolymers (Fig. 12a).

The flow temperatures were lower than the melting temperatures of the starting unit, i.e., the TΦB-monomethyl ester. The long SS gave rise to a lowering of the TΦB segments' melting temperatures. The flow temperature of the tri-block was higher than that of the multi-block copolymer despite the fact that the TΦB-monomethyl ester had a lower T_m (316 °C) than the TΦT-dimethyl ester (371 °C). This suggests that the decrease in the HS melting temperature was less significant when only one side was coupled; an effect for which the Flory relationship does not account. The modulus at 30 °C increased strongly with increasing amide content. A linear relationship was obtained between the TΦB content and the (log) modulus (Fig. 12b).

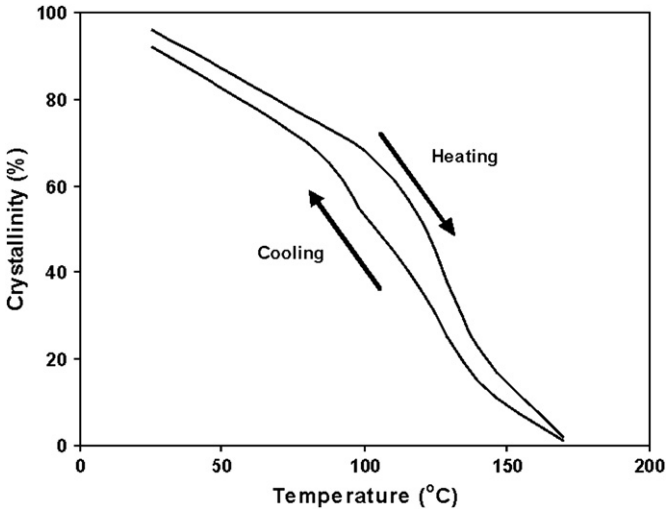

Fig. 10. The crystallinity of TΦB (**2d**) (heating and cooling curves) calculated from IR bands at 1643 and 1686 cm^{-1}.

The $PTMO_{1000}$ or $PTMO_{2900}$ series displayed the same trend. The increase in modulus with HS content was strong due to the reinforcing effect of the high aspect ratio, ribbon-like HS crystallites [12,17,19]. As a result, these systems could be regarded as nano-fiber reinforced composites. Also the molecular weight of the copolymer had little effect. The moduli of the tri-block copolymers were higher than those of the similar multi-block copolymers [30], particularly at low HS contents. However, this difference vanished at an HS content of approx. 20 wt.%, at which the difference in molecular weight between the tri- and the multi-block copolymers was the largest. The higher storage modulus of the tri-block copolymer was possibly due to a higher aspect ratio of the crystallites [12]. However, it is not clear why this would be the case only at low HS contents. The DMA results of the tri- and multi-block copolymers with 3 wt.% of HS were illustrative of the difference in the behaviour of the block copolymers (Fig. 13).

The low temperature behaviour of the tri- and multi-block copolymers seemed to be similar, whereas a large difference could be seen for the modulus at and above room temperature as well as for the melting transition, in that the tri-block copolymer displayed significantly higher values than its multi-block counterpart.

3.6. Melt rheology (dynamic test)

The rheological properties of the copolymer were measured using an oscillatory shear rheometer with parallel-plate geometry in the frequency range of 0.1–100 s^{-1} at 160 °C. The storage modulus and the loss modulus in the linear viscoelastic region of tri-block **2d** ($\eta_{inh} = 1.4$) and the multi-block copolymer ((–(PTMO–T)$_{10,000}$–TΦT)$_n$–) ($\eta_{inh} = 2.3$) are shown in Fig. 14.

In both cases, the concentration of the hard segment was kept at 3 wt.%. It can be seen from the graph that the tri-block copolymer displayed a decrease in modulus (G' and G'') upon decreasing the oscillation frequency. Moreover, at low frequency, a crossover point was apparent for the tri-block copolymer, at which the tan δ (G''/G') had the value of one. This point was thus regarded as the onset of gel formation [40]. The gelled structure here is a physical crosslinking due to the aggregation of the diamide endgroups. At low frequencies, the tan δ values were much lower than one, i.e., the elastic behaviour (G') was well above the viscous behaviour (G''). The melt was thus considered elastic since the elastic response exceeded the viscous response. At the same time, at low frequencies, the storage and loss moduli were less frequency dependent. A high G' with a small terminal slope suggested that there was a clustering of the amide end segments in the molten state leading to an network structure of the HS in the melt [41–43]. Contrarily to the tri-block copolymer, the G' and G'' curves for the multi-block copolymer decreased very sharply with frequency without crossing each other. Also, the non-existence of a plateau with a high terminal slope confirmed that there was no "crosslinking" of the copolymer in the melt taking place. The complex viscosity (η^*) of a tri-block and multi-block copolymer as a function of frequency can be seen in Fig. 15.

As the shear frequency decreased, the complex viscosity increased more significantly for the tri-block as opposed to the multi-block copolymer (both with 3 wt.% HS). Such an effect has been explained as being due to the formation of ordered structures in the melt [42]. The shape and slope of the complex viscosity curve for the multi-block copolymer corresponded to that of a high

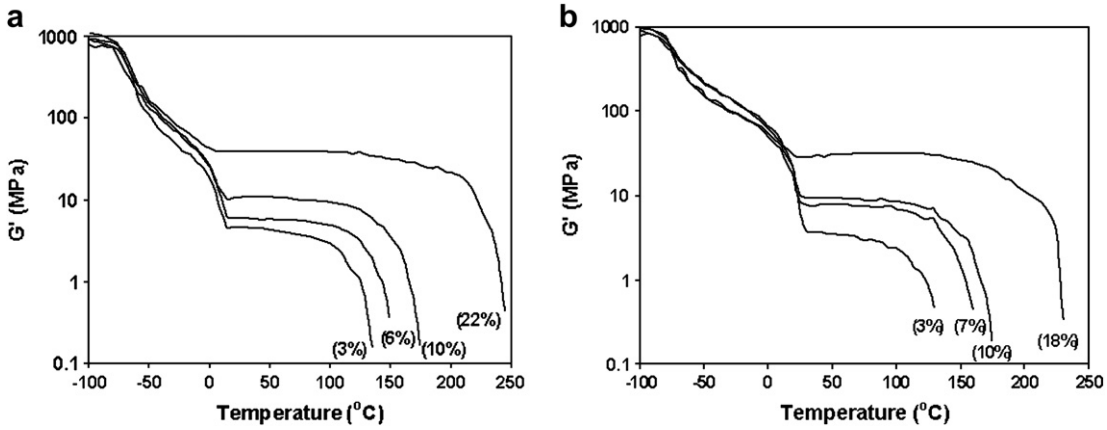

Fig. 11. The storage modulus curve of (a) the $PTMO_{1000}$- and (b) the $PTMO_{2900}$-based polymers (HS weight percentage is presented in the bracket).

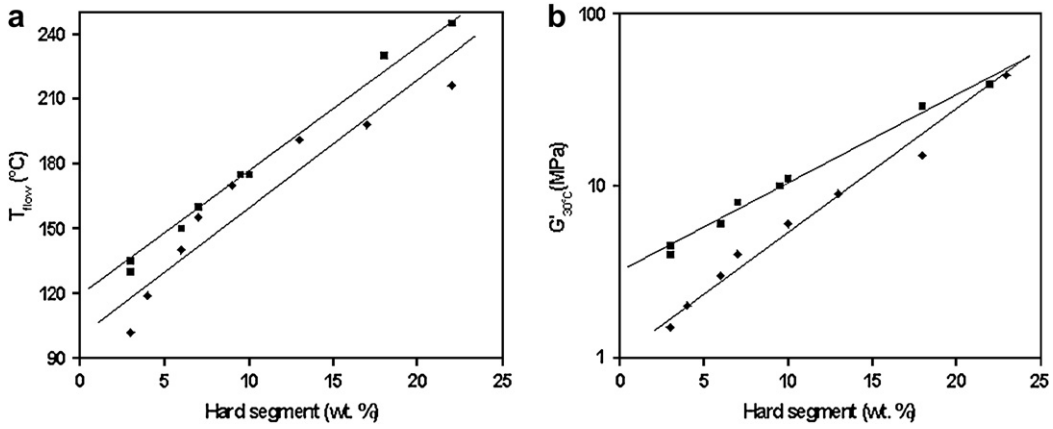

Fig. 12. (a) T_{flow} and (b) G' as functions of the amide content for the tri-block (■) and multi-block [30] (◆) copolymers.

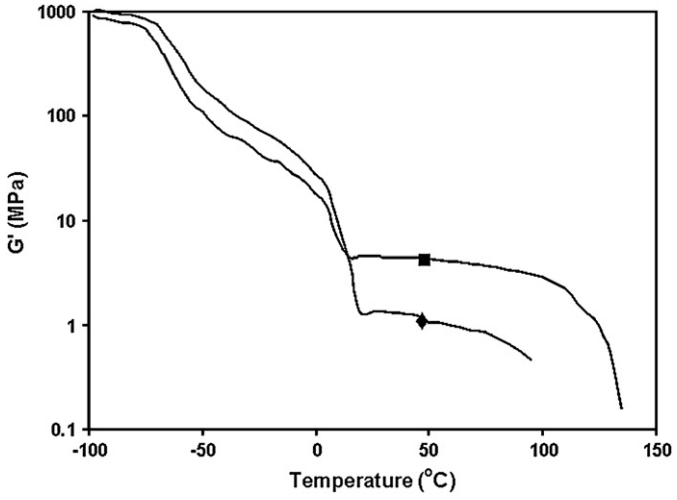

Fig. 13. The storage modulus as a function of temperature for tri-block (■) and multi-block [30] (◆) copolymers with 3 wt.% of HS.

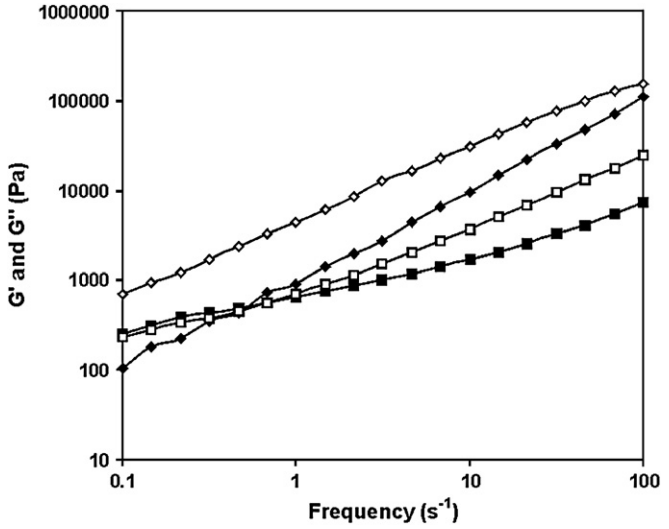

Fig. 14. The melt rheological behaviour of tri-block (**2d**) and multi-block copolymers with 3 wt.% HS as a function of frequency at 160 °C: ■, G' tri-block; □, G'' tri-block; ◆, G' multi-block; ◇, G'' multi-block.

molecular weight polymer with no (or insufficient) aggregation in the melt. The polyether segments on the amide mid-segments hindered the clustering of the amide segments [24]. End segments can form supramolecular structures [44]. In the tri-block copolymer, the end segments could aggregate (cluster) and form a weak network structure. Similar observations were obtained for all other copolymers in the series.

4. Conclusions

The mono-functional diaramide hard segment TΦB of high purity was synthesized and subsequently characterized by NMR, IR and MALDI-TOF. Tri-block copolymers with varying concentrations of mono-functional hard end segments were then prepared and

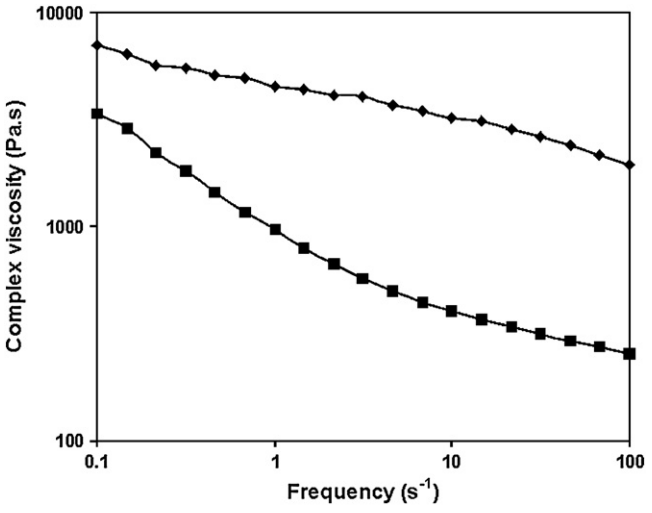

Fig. 15. The complex viscosity of a tri-block ($\eta_{inh} = 1.4$) (■) and multi-block ($\eta_{inh} = 2.3$) (◆) copolymer with 3 wt.% HS as a function of frequency at 160 °C.

analyzed by IR, NMR and DSC. The rate of crystallization of the hard end segments was found to be very high as was their crystallinity (~95%). The HS of the tri-block copolymers had a nano-ribbon crystallite structure with a high aspect ratio (>500), and the system could be regarded as a nano-fiber reinforced composite. The modulus and the flow temperature of the copolymer increased strongly with the HS content. The storage modulus of tri-block copolymer was higher than that for the similar multi-block copolymer and particularly at low contents of hard end segment. The flow temperature of the tri-block was ~20 °C higher than that for the multi-block copolymer.

The rheological behaviour of the tri-block copolymers was explored and was found to be very unusual. The low molecular weight tri-block copolymers displayed very low melt viscosities at high frequency, whereas the melt behaved as a gel at low frequency. The network structure in the melt was probably a result of molten clustered amide end segments. It was striking that the network forming effect was observed for the tri-block copolymers and not for the multi-block copolymers. Apparently the mono-functional end blocks were able to cluster better than the mid-blocks.

Acknowledgement

This work is part of the research programme of the Dutch Polymer Institute (DPI), project nr. 479.

References

[1] Holden G, Legge NR, Quirk RP, Schroeder HE. Thermoplastic elastomers. 2nd ed. Munich: Hanser Publishers; 1996.
[2] Bates FS, Fredrickson GH. Phys Today 1999;52(2):32–8.
[3] Allen WT, Eaves. Angew Makromol Chem 1977;58/59:321.
[4] Kim I, White JL. J Appl Polym Sci 2003;90(14):3797–805.
[5] Fakirov S. Handbook of condensation thermoplastic elastomers. New York: Wiley Publishers; 2005.
[6] Harrell LJ. Macromolecules 1969;2:607–12.
[7] Eisenbach CD, Baumgartner M, Guenter C. In: Lai J, Mark JE, editors. Advances in elastomer and rubber elasticity. New York: Plenum; 1986.
[8] Eisenbach CD, Nefzger H. In: Cumbertson WM, editor. Multiphase macromolecular systems. Contemporary topics in polymer science, vol. 6. New York: Plenum; 1989.
[9] Gaymans RJ, de Haan JL. Polymer 1993;34:4360–4.
[10] Niesten M, Feijen J, Gaymans RJ. Polymer 2000;41(24):8487–500.
[11] Krijgsman J, Feijen J, Gaymans RJ. Polymer 2004;45(14):4685–91.
[12] van der Schuur M, de Boer J, Gaymans RJ. Polymer 2005;46(22):9243–56.
[13] Sheth JP, Klinedinst DB, Wilkes GL, Yilgor I, Yilgor E. Polymer 2005;46:7317–22.
[14] Klinedinst DB, Yilgor E, Yilgor I, Beyer FL, Sheth JP, Wilkes GL. Rubber Chem Technol 2005;78:737–53.
[15] Versteegen RM, Sijbesma RP, Meijer EW. Macromolecules 2005;38:3176–84.
[16] Versteegen RM, Kleppinger R, Sijbesma RP, Meijer EW. Macromolecules 2006;39:772–83.
[17] Biemond GJE, Feijen J, Gaymans RJ. J Appl Polym Sci 2007;105(2):951–63.
[18] Hesken D, Feijen J, Gaymans RJ. J Polym Sci Part A Polym Chem 2007;45(19):4522–35.
[19] Sauer BB, McLean RS, Gaymans RJ, Niesten MCJE. J Polym Sci Part B Polym Phys 2004;42(9):1783–92.
[20] Sijbesma RP, Beijer FH, Brunsveld L, Folmer AJB, Hirschberg Ky, Lange RFM, et al. Science 1997;278:1601–4.
[21] Yamauchi K, Kanomata A, Inoue T, Long TE. Macromolecules 2004;37(10):3519–22.
[22] Kautz H, van Beek DJM, Sijbesma RP, Meijer EW. Macromolecules 2006;39(13):4265–7.
[23] Folmer BJB, Sijbesma RP, Versteegen RM, van der Rijt JAJ, Meijer EW. Adv Mater 2000;12(12):874–8.
[24] Van Beek DJM, Spiering AJH, Peters GWM, te Neijenhuis K, Sijbesma RP. Macromolecules 2007;40(23):8464–75.
[25] Lange RFM, Van Gurp M, Meijer EW. J Polym Sci Part A Polym Chem 1999;37(19):3657–70.
[26] Ojelund K, Loontjens T, Steeman P, Palmans A, Maurer F. Macromol Chem Phys 2003;204(1):52–60.
[27] Lillya CP, Baker RJ, Hutte S, Winter HH, Lin YG, Shi JF, et al. Macromolecules 1992;25(8):2076–80.
[28] Colombani O, Barioz C, Bouteiller L, Chaneac C, Fomperie L, Lortie F, et al. Macromolecules 2005;38(5):1752–9.
[29] Niesten M, Gaymans RJ. Polymer 2001;42(14):6199–207.
[30] Niesten M, ten Brinke JW, Gaymans RJ. Polymer 2001;42(4):1461–9.
[31] Krijgsman J, Husken D, Gaymans RJ. Polymer 2003;44(25):7573–88.
[32] Gaymans RJ, Harkema S. J Polym Sci Part B Polym Phys 1977;15:587–90.
[33] Wunderlich B. Thermal analysis of polymeric materials. Heidelberg: Springer; 2004.
[34] Nadkarni VM, Bulakh NN, Jog JP. Adv Polym Technol 1993;12:73–9.
[35] Roerdink E, Warnier JMM. Polymer 1985;26:1582–8.
[36] Koning C, Buning GW. Recent Res Dev Macromol Res 1999;4:1.
[37] Bouma K, Gaymans RJ. Polym Eng Sci 2001;41:466–74.
[38] van Bennekom ACM, Gaymans RJ. Polymer 1997;38:657–65.
[39] Flory PJ. Trans Faraday Soc 1955:848–57.
[40] Schramm G. A practical approach to rheology and rheometry. Hakke Publishers; 1994.
[41] Yang IK, Tsai PH. Polymer 2006;47:5131–40.
[42] Wang Y, Zhao Q, Liu M, Wang Z, Liu Y, Cao S, et al. J Appl Polym Sci 2005;98:1643–51.
[43] I-Kuan Yang, Ping-Hung Tsai. J Polym Sci Part B Polym Phys 2005;43:2557–67.
[44] Biemans HAM, Rowan AE, Verhoeven A, Vanoppen P, Latterini L, Foekema J, et al. J Am Chem Soc 1998;120(43):11054–60.